THE SOMETHING SURVEY: ANALYZING THE EVOLUTION OF MGII ABSORBERS

NIGEL L. MATHES[1], CHRISTOPHER W. CHURCHILL[1], AND MICHAEL T. MURPHY[2]

Draft version March 23, 2016

ABSTRACT

We present a detailed measurement of the redshift number density of MgII absorbers as measured in archival VLT/UVES and Keck/HIRES spectra. This survey examines 432 VLT/UVES spectra from the UVES SQUAD collaboration and 170 Keck/HIRES spectra from the KODIAQ group, allowing for detections of MgII absorbers from $0.08 < z < 2.57$. We employ an accurate, automated approach to line detection which consistently detects absorption lines with equivalent widths $W_r < 0.02$ in $S/N = 40$ spectra. We then measure the equivalent widths, apparent optical depth column densities, and velocity widths for each absorbing system. This results in a complete sample of strong ($W_r > 0.3$) and weak ($Wr < 0.3$) MgII absorbers, allowing for accurate determination of the number density of these absorbers across cosmic time. Preliminary results show power-law behavior for the MgII equivalent width distribution function down to small equivalent widths, implying self-similar absorbing structures. This power law is smooth and shallow at low redshifts ($z < 1.5$), but has a kink at redshifts between $1.5 < z < 2.5$ due to an excess of strong absorbers compared to weak absorbers. These trends seem to follow our general idea of the history of cosmic metal enrichment, with an evolutionary transition occurring around the time of the global star formation peak of the universe.

Keywords: galaxies: halos — quasars: absorption lines

1. INTRODUCTION

One of the most important questions in modern studies of galactic evolution asks, how do baryons cycle into and out of galaxies, and how does this cycle determine the growth and evolution of galaxies themselves? More specifically, how does the process of gas accretion, star formation, and subsequent supernovae driven feedback shape both the galaxy itself and the circumgalactic medium (CGM) surrounding the galaxy? By using spectroscopic observations of quasars, we can identify and analyze metal line absorbers in the halos of foreground galaxies.

Perhaps one of the most prolific absorption featues, the Mg II $\lambda\lambda 2796, 2803$ doublet, traces cool ($T \simeq 10^4$ K) metal enriched gas in the disks and halos of galaxies. It is one of the best tracers of this gas because it can exist in a wide range of ionizing conditions, it is observable in optical wavelengths from redshift $0.1 < z < 2.5$, and it has predictable line characteristics defined by its resonant doublet nature which make it ideal for automated searches.

Many surveys have been undertaken to inventory the cosmic nature of intervening Mg II absorbers. The earliest of those (Lanzetta et al. 1987; Tytler et al. 1987; Sargent et al. 1988; Steidel & Sargent 1992) found that Mg II systems with rest equivalent widths above 0.3 show show now evolution in $\frac{dN}{dZ}$ between redshifts $0.2 < z < 2.15$, with $\frac{dN}{dZ}$ increasing slowly with redshift. These studies also found that the equivalent width distribution function, $f(w)$, could be fit equally well with either an exponential or a power law, leaving to question whether the cosmic distribution of Mg II in galactic halos exhibited a fractal, self-similar nature, or if there was a physical limit to size scale and quantity of Mg II absorbing gas.

More modern surveys have taken one of two different approaches to try to DO SOMETHING ABOUT MGII. Churchill et al. (1999) and Narayanan et al. (2007) aimed to analyze the behavior of weak ($W_r(2796) < 0.3$) Mg II absorbers. They find that $\frac{dN}{dZ}$ rises smoothly from $0 < z < 1.4$, but then decreases rapidly around $z \simeq 2$. In addition, the equivalent width distribution function for weak absorbers is best fit by a power law, strongly disfavoring an exponential fit. The implication here is that these weak absorbers, tracing smaller, less kinematically spread Mg II systems, exhibit self-similar behavior in the halos of galaxies and potentially evolve away relative to stronger Mg II absorbing systems at redshifts near the cosmic SFR peak.

The most modern studies employ new multi-object spectrographs such as the Sloan Digital Sky Survey (SDSS) and the FIRE spectrograph on the Magellan Baade Telescope (Nestor et al. 2005; Matejek & Simcoe 2012). These surveys aim to use massive quantities of quasar spectra in order to remove uncertainties in the distribution of strong intervening absorbers. Nestor et al. (2005), examining over 1300 Mg II absorbers with $W_r(2796) > 0.3$, find that the equivalent width distribution function is well fit by an exponential. They do not find evidence for redshift evolution in systems with $0.4 < W_r(2796) < 2$, but see a decrease in the number of lines stronger than $W_r(2796) > 2$ with decreasing redshift, towards $z < 1$. Matejek & Simcoe (2012), looking at 111 Mg II absorbing systems from $1.9 < z < 6.3$, find that the equivalent width distribution function is well fit by an exponential. They do note, however, that $f(W)$ does steepen at redshifts below $z = 3$, implying some causal connection between the $f(W)$ and the cosmic SFR peak. They also observe that systems with $W_r(2796) < 1.0$ show no evolution with redshift, but stronger systems increase nearly three-fold in $\frac{dN}{dZ}$ from low redshift to $z \simeq 3$.

For our survey, we aim to analyze largest, most comprehensive sample of high resolution, high signal-to-noise quasar spectra to uniformly observe both strong and weak Mg II absorbers. We hope to finally rectify the discontinuities in prior Mg II absorption line surveys. To do so, we will examine 602 quasar spectra spanning emission redshifts from SOMETHING to SOMETHING observed with either the VLT/UVES or KECK/HIRES spectrographs. We detect

[1] New Mexico State University, Las Cruces, NM 88003
[2] Swinburne University of Technology, Victoria 3122, Australia

over 1200 Mg II absorbing systems from $0.14 < z < 2.63$ to a detection limit of $W_r(2796) \simeq 0.02$ in $\frac{S}{N} = 40$ spectra. We aim to characterize the evolution in the number density of all Mg II absorbers from present to beyond the peak of the cosmic star formation rate.

We begin by explaining the methods of acquiring and analyzing the quasar spectra in section 2. Next, in section 3, we present the results showing the evolution of the Mg II equivalent width distribution, $\frac{dN}{dX}$, and the Mg II column density distribution across redshift. In section 4 we analyze the funcitonal fit to the column density distribution and derive the relative matter density contributed to the universe by Mg II, $\Omega_{\mathrm{Mg II}}$. In Section 5 we summarize our results and look to future studies using this rich data set, including a companion analysis of intervening C IV absorbers and detailed kinematic analysis of intervening absorbing systems. For all calculations, we adopt the most recently published Planck cosmology, with $H_0 = 67.74$ kms^{-1}Mpc, $\Omega_M = 0.258$, and $\Omega_\Lambda = 0.742$.

2. DATA AND ANALYSIS

2.1. *Quasar Spectra Sample*

We have assembled a sample of 602 archival quasar spectra observed with the VLT/UVES and KECK/HIRES spectrographs. The data originates from two archival data mining efforts - the UVES Squad collaboration (432 spectra) led by Michael Murphy, and the KODIAQ Survey (170 spectra) led by John O'Meara (O'Meara et al. 2015). The spectra range in signal-to-noise from *XXX* to *YYY*, quasar emission redshifts span *XXX* $< z <$ *YYY*, and wavelength coverage for each spectrum spans either $3000 - 6600$ or $3000 - 10,000$, depending upon whether the red arm of each spectrograph was used.

2.2. *Continuum Fitting and Line Detection*

The KODIAQ data sample is reduced and fully continuum fit, delivered as normalized spectra according to the prescriptions of O'Meara et al. (2015). The UVES Squad sample also comes reduced, but with an automatic, low order polynomial continuum fit applied. This fith can incorrectly estimate the continuum around narrow emission regions and broad absorption features. For the UVES data sample, I add a higher order continuum fit to difficult regions of the spectra. We use UVES_popler, an ESO/VLT UVES post-pipeline echelle reduction program written by Michael T. Murphy (Copyright 2003-2015 Michael T. Murphy) to apply these fits, preserving continuity of the continuum with non-absorbing regions.

The next step involves detecting all Mg II absorption features. We first limit the search range to regions of the spectrum redward of the Lyα emission, as Lyα forest contamination would render automatic detection of weaker metal lines nearly impossible. We also do not search 5000 km s^{-1} blueward of the quasar emission redshift in order to avoid absorbers associated with the quasar itself. Finally, we exclude regions of strong telluric absorption bands, specifically from $6277 - 6318$, $6868 - 6932$, $7594 - 7700$, and $9300 - 9630$, finding that the molecular line separations and ratios can lead to numerous false positives when searching for Mg II doublets.

To find all intervening Mg II $\lambda\lambda2796, 2803$ absorbers, we employ a techinque outlined in Zhu & Ménard (2013), in which we perform a matched filter search for absorption candidates detected above a certain signal-to-noise (S/N) threshold. The filter is a top hat function centered at the wavelength of the desired redshifted absorption line. Its width is selected

to match the resolution of the spectrograph used (VLT/UVES $\simeq 40,000$; KECK/HIRES $\simeq 45,000$), set as the FWHM of an unresolved gaussian absorption feature. We convolve the filter with the normalized spectrum to generate a normalized power spectrum in redshift space, with absorption features having positive power.

Because the error spectrum in both instruments is complicated and often discontinuous, we cannot convolve the filter with the errors to derive normalized noise estimates. Instead, we examine the noise in the derived power spectrum. We sigma clip chunks of the power spectrum before calculating its standard deviation. We take this measurement as the noise and require a detected line have a derived $S/N > 5\sigma$. A confirmed doublet detetection for Mg II $\lambda\lambda2796, 2803$ requires detection of $S/N_{2796} > 5\sigma$ and $S/N_{2803} > 3\sigma$. In addition, in our automated routines we remove detections with non-physical doublet ratios in unsaturated regions; specifically, we exclude cases where $W_r(2803) > W_r(2796)$ and $W_r(2803) < 0.3 \times W_r(2796)$. We relax this constraint in saturated lines.

All absorption features are visually verified upon completion of the detection algorithm. Multiple feature detections within ±500 km s^{-1} of each other are grouped together to generate absorption systems to be analyzed. Once absorption systems are identified, we calculate the optical depth-weighed mean absorption redshift to define the center of the entire absorption system.

We also derive an equivalent width detection limit across the spectrum. To do so, we assume gaussian features and calculate the full-width at half-max (FWHM) defined by the resolution of the instrument and the height of the gaussian defined by the derived error spectrum. We then integrate to find the equivalent width, and take that value as the minimum detectable equivalent width. This full equivalent width detection limit spectrum will allow us to accurately characterize the completeness of our sample, along with the full redshift path length searched.

2.3. *Measuring Absorption Properties*

For each absorption system, we automatically define the wavelength bounds of each absorbing region by finding where 3 pixels of the absorption trough recover past the 1σ error level in the spectrum., Within these regions we calculate equivalent widths (W_r), velocity widths (Δv), kinematic spreads (Ω_v), apparent optical depth (AOD) column densities ($log(N)$), and absorption asymmetries.

3. RESULTS

3.1. *Sample Characterization*

Distributions for MgII absorbers. Histograms of redshfit, EW, logN, velocity spread.

3.2. *dN/dZ and dN/dX*

Previous studies of the statistical properties of Mg II absorbers have been forced to focus either on strong or weak absorbers. The largest sample of quasar spectra originates from the Sloan Digital Sky Survey (SDSS), which employs a spectrograph with an instrumental resolution around 69 km s^{-1}, limiting SDSS absorption surveys to strong absorbers (Zhu & Ménard 2013; Cooksey et al. 2013) (MORE CITATIONS). Conversely, previous studies of weak absorbers used small samples of quasar spectra, never exceeding 50 quasar spectra (Kacprzak et al. 2011) (MORE CITATIONS). In this pa-

per, we aim to characterize the evolution of the incidence rate, number density per absorption path length, and cosmic mass density of all Mg II absorbers above a detection limit of $W_r(2796) > 0.02$ from redshifts $0.18 < z < 2.5$.

The number density of Mg II absorbers per redshift path length and its associated variance is defined as

$$\frac{dN}{dZ} = \sum_i \frac{1}{\Delta Z(W_r^i)}, \quad \sigma_{\frac{dN}{dZ}}^2 = \sum_i \left[\frac{1}{\Delta Z(W_r^i)}\right]^2, \quad (1)$$

where we count the number of Mg II absorbers, dividing by the total searched redshift path length (ΔZ), defined as

$$\Delta Z(W_r^i) = \int_{z_0}^{z_1} g(W_r^i, z)\, dz, \quad (2)$$

where $g(W_r, z)$ is the equivalent width sensitivity function. Equation (6) in Lanzetta et al. (1987) defines $g(W_r, z)$, which counts the number of spectra in which a given equivalent width absorption feature may be detectected at the 5σ level in a given redshift interval.

The number density of Mg II absorbers per absorption path and its associated variance is defined as

$$\frac{dN}{dX} = \sum_i \frac{1}{\Delta X(W_r^i)}, \quad \sigma_{\frac{dN}{dZ}}^2 = \sum_i \left[\frac{1}{\Delta X(W_r^i)}\right]^2, \quad (3)$$

where we count the number of Mg II absorbers, dividing by the total searched absorption path (ΔX), defined as

$$\Delta X(W_r^i) = 2\sqrt{\Omega_M(1+\Delta Z)^3 + \Omega_\Lambda}/(3\Omega_M), \quad (4)$$

where Ω_M is the cosmic matter density, and Ω_Λ is the cosmic density attributed to dark energy.

In Figure 3, we plot $\frac{dN}{dX}$ as a function of redshift for varying equivalent width cuts. Dotted lines are fit according to the analytical form which allows for redshift evolution in $\frac{dN}{dX}$, defined as,

$$\frac{dN}{dX} = n\sigma(1+z)^\epsilon, \quad (5)$$

where n is the number density of Mg II absorbers, σ is the absorbing cross-section, and ϵ is the power dependence of $\frac{dN}{dX}$ on redshift. We find that the best-fit value of ϵ increases with increasing equivalent width cuts, with the distribution showing a steeper dependence on redshift as we observe larger and more complex Mg II absorbing systems. This trend is driven primarily by an enhancement in $\frac{dN}{dX}$ for the strongest Mg II absorbers around $z = 2$, relative to lower redshifts. We suspect that the correlation between this enhancement and the cosmic SFR peak is not coincidence, and that these stronger Mg II absorption systems are direct byproducts of star formation driven winds in this same epoch.

3.3. *Equivalent Width Distribution*

To calculate the equivalent width distribution, we calculate $\frac{dN}{dX}$ for each absorber equivalent width, sum the distribution in equivalent width bins, and then divide by the bin width. The result is a characteristic number density of Mg II absorbers per absorption path length as a function of their equivalent width.
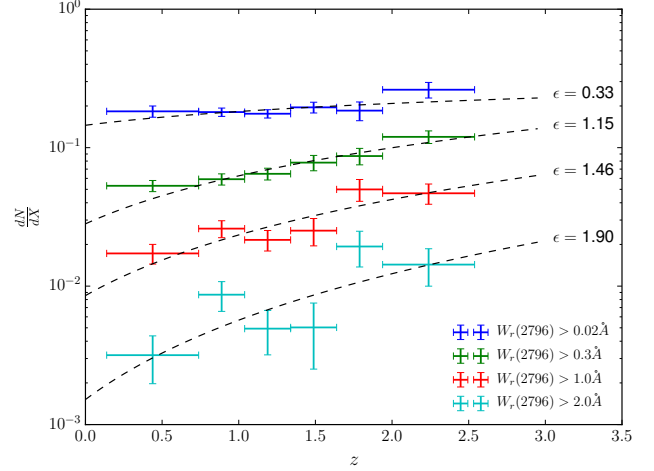

Figure 1. $\frac{dN}{dX}$ as a function of redshift for varying $W_r(2796)$ cuts. Colors represent different equivalent width cuts. The black dotted lines are fits to the distribution of the functional form $f(z) = n\sigma(1+z)^\epsilon$, with the best fit ϵ value labelled. We see increasing values of ϵ with increasing equivalent width, driven by an enhancement of stronger Mg II absorbers around redshift 2 compared to lower redshifts.

3.4. *Column Density Distribution*

To calculate the column density distribution, we calculate $\frac{dN}{dX}$ for each absorber equivalent width, sum the distribution in column density bins, and then divide by the bin width. The result is a characteristic number density of Mg II absorbers per absorption path length as a function of their column densities. It should be noted that at high column densities near $\log(N(MgII)) = 15$, the measured column densities are lower limites as the AOD method to measure column densities cannot constrain the true col

4. DISCUSSION

4.1. *Evolution of MgII Distributions*

Narayanan et al. (2007) measure the evolution of weak Mg II absorbers from $0.4 < z < 2.4$ in VLT/UVES spectra. They compare to Churchill et al. (1999), which fits the equivalent width distribution with a power law, and to Nestor et al. (2005), which fits an exponential to $f(W_r)$. In the case of weak absorbers at $z < 1.4$, Narayanan et al. (2007) finds that a power law with a slope of $\alpha = -1.04$ is a satisfactory fit, mirroring the results from Churchill et al. (1999). However, when examining the higher redshift half of their sample, they find a decreased number of weak Mg II absorbers and prefer the exponential fits of Nestor et al. (2005). Unfortunately, they do not also entertain the thought that a shallower power law slope, such as $\alpha = -0.8$, also accurately characterizes the equivalent width distribution of weak Mg II absorbers.

Narayanan et al. (2007) also analyze the evolution of $\frac{dN}{dZ}$ with redshift for weak Mg II absorbers. They find that the distribution follows the classical "no evolution" assumption, that is the expected number density for a nonevolving population of absorbers in a ΛCDM universe, at redshifts less than $z = 1.5$. At higher redshift, they find the number density of weak absorbers decreases. Here, in our study, we find similar behavior for absorbers with $0.02 \leq W_r(2796) < 0.3$, except we observe the relative decrease in $\frac{dN}{dZ}$ occurring around $z = 1$.
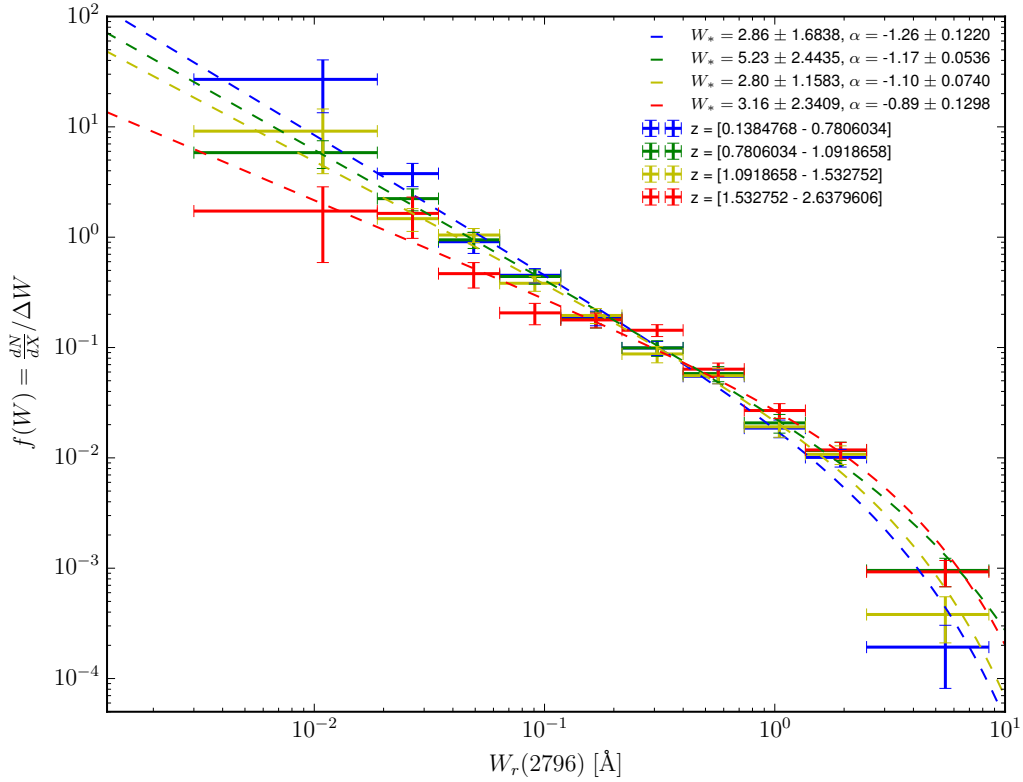
Figure 2. The equivalent width distribution of Mg II absorbers, defined as the comoving line density ($\frac{dN}{dX}$) in each equivalent width bin divided by the bin width. We fit this distribution with a Schechter function, capturing the self-similar power law behavior of the distribution before the exponential cutoff limiting the size of Mg II absorbers.

Steidel & Sargent (1992), and later Churchill & Vogt (2001), examine the redshift evolution of $\frac{dN}{dZ}$ for strong Mg II absorbers with $W_r(2796) > 0.3$. They find that the number density of strong Mg II absorbers increases from $z = 0$ to $z = 2.2$, however they cannot derive the slope of this trend to sufficient accuracy to distinguish between an evolving population or a non-evolving population. Performing a similar analysis on our sample, and taking absorbers with $W_r(2796) > 0.3$, we find that a fit with a slope of $\alpha = SOMETHING$ is appropriate, implying that the number density of strong Mg II absorbers does indeed evolve, with more strong absorbers appearing around $z = 2$.

Kacprzak & Churchill (2011) attempted to combine many previous studies to accurately characterize the equivalent width distribution function. They find a Schechter function with a characteristic normalization, low equivalent width slope, and exponential cutoff best fit the data. SAY SOMETHING AND COMPARE.

4.2. *Omega_MgII*

We now aim to calculate the matter density of Mg II absorbers across cosmic time. To do so, we emply the following equation,

$$\Omega_{MgII} = \frac{H_0 \, m_{Mg}}{c \, \rho_{c,0}} \int_{N_{min}}^{N_{max}} f(N_{MgII}) N_{MgII} \, dN_{MgII}, \quad (6)$$

where H_0 is the Hubble constant today, $m_{Mg} = 4.035 \times 10^{-23}$ g, c is the speed of light, $\rho_{c,0}$ is the critical density at

present, $f(N_{MgII})$ is the column density distribution of MgII absorbers, and N_{MgII} is the column density. Using our derived fit to the column density distribution, we are able to numerically integrate the first moment from $0 < N(MgII) < 20 \, \text{cm}^{-2}$. The results are shown below in Figure 4.

Errors are derived by bootstrap Monte-Carlo. We pick at random with replacement column densities from the sample of measured column densities for all of our Mg II absorbers. We then recalculate the column density distribution, find the best parameterized Schechter fit, and then integrate and compute Equation 6. We take the standard deviation about the mean of this ensemble of simulated measurements as the error in Ω_{MgII}.

5. CONCLUSIONS

Stuff.

- Things

- More things

- Potentially some more stuff here

Acknowledgements.

REFERENCES

Churchill, C. W., Rigby, J. R., Charlton, J. C., & Vogt, S. S. 1999, ApJS, 120, 51

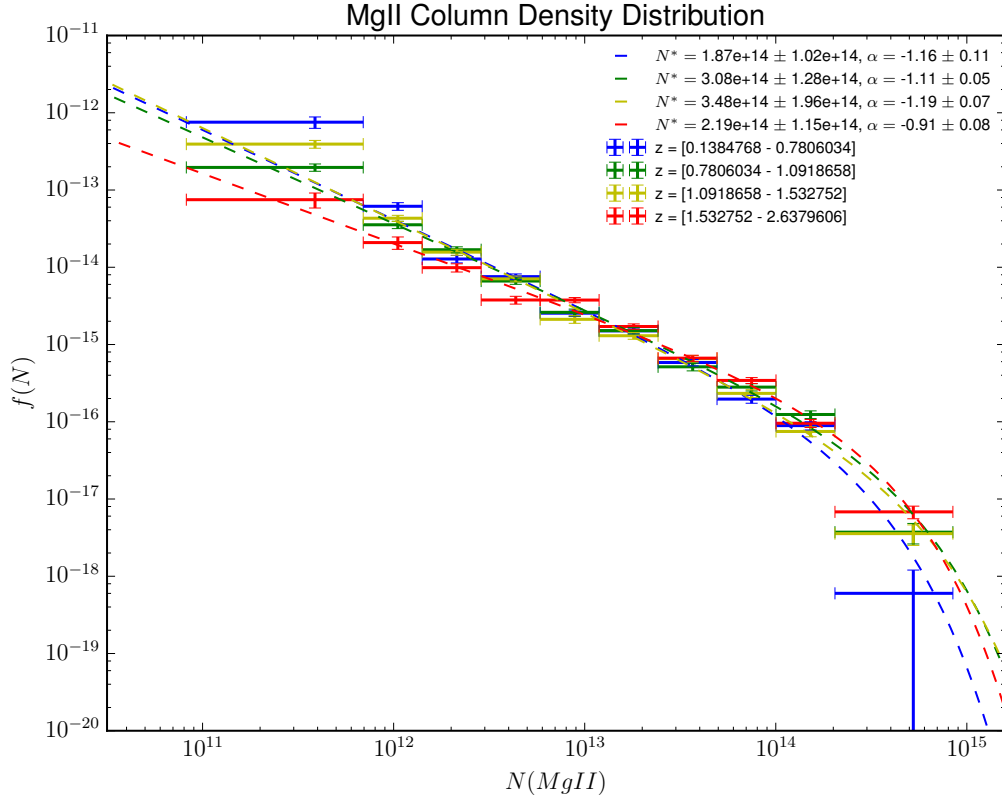Churchill, C. W., & Vogt, S. S. 2001, AJ, 122, 679

Figure 3. The column density distribution of Mg II absorbers, defined as the comoving line density in each column density bin divided by the bin width. We fit this distribution with a Schechter function.

Cooksey, K. L., Kao, M. M., Simcoe, R. A., O'Meara, J. M., & Prochaska, J. X. 2013, ApJ, 763, 37

Kacprzak, G. G., & Churchill, C. W. 2011, ApJ, 743, L34

Kacprzak, G. G., Churchill, C. W., Evans, J. L., Murphy, M. T., & Steidel, C. C. 2011, MNRAS, 416, 3118

Lanzetta, K. M., Turnshek, D. A., & Wolfe, A. M. 1987, ApJ, 322, 739

Matejek, M. S., & Simcoe, R. A. 2012, ApJ, 761, 112

Narayanan, A., Misawa, T., Charlton, J. C., & Kim, T.-S. 2007, ApJ, 660, 1093

Nestor, D. B., Turnshek, D. A., & Rao, S. M. 2005, ApJ, 628, 637

O'Meara, J. M., Lehner, N., Howk, J. C., et al. 2015, AJ, 150, 111

Sargent, W. L. W., Steidel, C. C., & Boksenberg, A. 1988, ApJ, 334, 22

Steidel, C. C., & Sargent, W. L. W. 1992, ApJS, 80, 1

Tytler, D., Boksenberg, A., Sargent, W. L. W., Young, P., & Kunth, D. 1987, ApJS, 64, 667

Zhu, G., & Ménard, B. 2013, ApJ, 770, 130

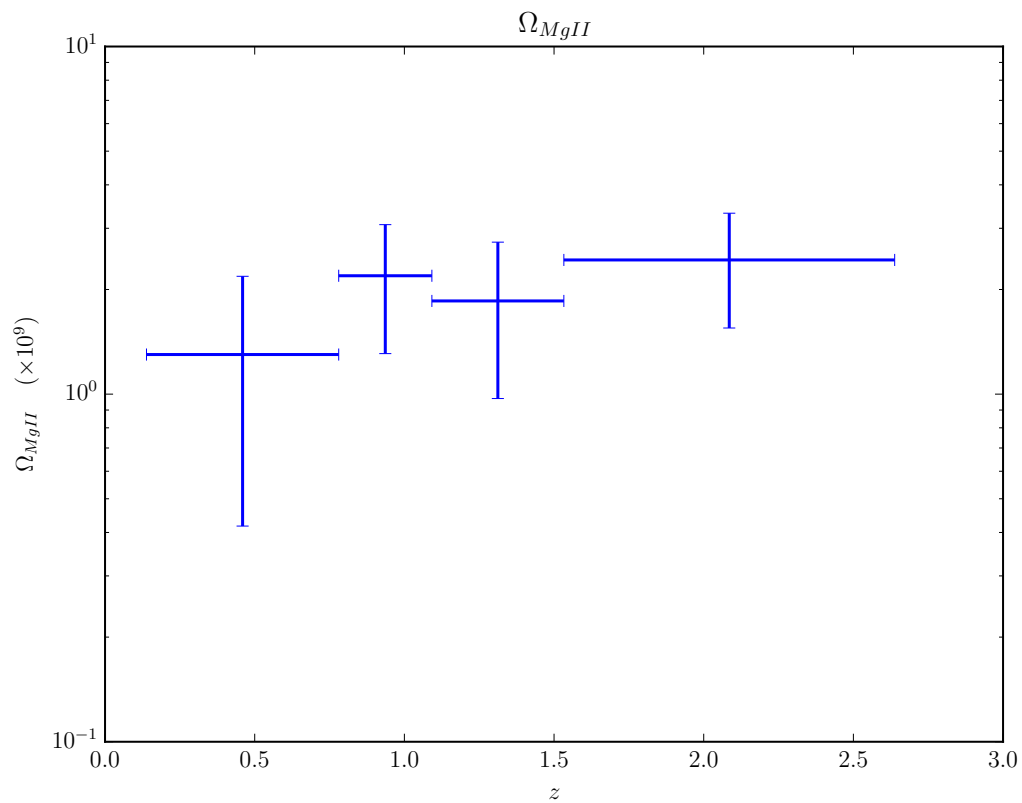**Figure 4.** $\Omega_{\mathrm{Mg\,II}}$ as a function of redshift. The cosmic mass density of Mg II stays roughly flat near a value of 1×10^{-9}, with a potential increase from $z = 0.1$ to $z = 2.5$.